AIAA JOURNAL
Vol. 48, No. 6, June 2010

# Technical Notes

## Near-Field Acoustic Characteristics of a Turbulent Axisymmetric Pulsed Jet

Rajan Kumar,* Anjaneyulu Krothapalli,† and Isaac Choutapalli‡
*Florida State University, Tallahassee, Florida 32310*

DOI: 10.2514/1.J050026

### I. Introduction

PULSED jets have a variety of applications ranging form pulsing blood flow in the human heart (Gharib et al. [1]) to pulsed-detonation engines (PDEs). The first application of a pulsed-jet engine was during the World War II for propelling a flying/buzz bomb (Manganiello et al. [2]). Pulsed-jet engines are known to yield higher levels of thrust, light in weight and simple in design, and therefore have found interest in variety of applications such as radio controlled small aircraft to the vertical takeoff and landing aircraft. The pulsation is known to play an important role on the engine thrust performance. Theoretical analysis by Seikman [3] on a two-dimensional planar and Weihs [4] on an axisymmetric nozzle show that for the same nozzle exit mass flow, the average thrust of a pulsed jet is much higher than the equivalent steady jet. The present experiment is conducted in the context of a study on pulsed-jet ejectors that are shown to produce thrust augmentation ratio (total thrust/primary pulsed-jet thrust) of about 2 (Choutapalli et al. [5]). In a pulsed jet, the fluid ejected from the nozzle rolls up into a vortex ring, which in turn moves downstream (Fig. 1). When a jet is pulsed continuously, a sequence of large-scale structures or vortex rings is produced at regular intervals with jetlike flows in between.

In the context of jet mixing and far-field noise studies, many investigations have been carried out on acoustically exited jets with a focus on dynamics of the resultant coherent structures. A notable study by Crow and Champagne [6] generated small pulsation by forcing an axisymmetric steady jet using a loud speaker to produce coherent large eddies. The exit velocity of the jet was relatively constant and the pulsation was simply a perturbation to the flow. Hence, it may be considered as the perturbed jet. Here, the pulsed jet is referred to as one in which variation with time of the exit velocity is large and of the same order of magnitude as the mean exit velocity. Even though, the pulsed jet shows vortex rings similar to those of perturbed jets, they are much stronger resulting in a jet that has very different characteristics than those of a corresponding steady jet [7]. Most of the previous investigations on pulsed jets have been focused on the trust augmentation and associated turbulent vortex structures including the recent detailed investigation by Choutapalli et al. [5] and the references there in. Choutapalli et al. [5] provided a detailed understanding of the flow physics responsible for the increased thrust. Detailed flowfield analysis using particle image velocimetry (PIV) showed the evolution of vortices and their role in enhanced mass entrainment and mixing.

The connection between the large-scale structures and the far-field noise of a jet has been a subject of many studies and a summary can be found in Arakeri et al. [8]. Near-field microphone measurements, for example by Mollo-Christensen [9], have shown that pressure fluctuations arrive in rather well-defined wave packets, suggesting them to be associated with the well organized structures existing within the jet. It is also known that the presence of coherent vortical structures in supersonic jets operating at off design conditions (e.g. screeching jets) show a significant increase in the near-field sound pressure levels. Alkislar et al. [10] have shown that the near-field screech amplitude is related to the coherent vorticity strength. With these observations in mind, it is suggested that vortex rings in a pulsed jet will generate significant near-field pressure fluctuations which will result in increased overall sound pressure level (OASPL). Hooker and Rumble [11] have experimentally studied the noise of the rotating valve simulator to simulate the exhaust cycle of a pneumatic rock drill and reported the dependence of air supply pressure on the measured sound pressure levels. He and Karagozian [12] performed numerical simulations (quasi-1-D computations) on a number of nozzle shapes to study the effect of geometry on the performance and noise characteristics of a PDE. Most of their noise estimates were made inside the nozzle and in the jet centerline. In general, their estimates indicate that noise levels produced by convergent or divergent nozzles are slightly less than straight tubes. Shaw et al. [13] carried out acoustic measurements on a PDE being developed at the U.S. Air Force Research Laboratory's Propulsion Directorate. The tests were conducted with one of the four tubes of 1 in. diameter and the engine was fired at a pulsing frequency of 20 Hz. The measurements included a microphone array located at 13 diameters from the nozzle exit and the OASPL measured were in the range of 147 to 159 dB, depending upon the location of the microphone. However, little information exists in the literature on the near-field acoustic characteristics of a pulsed jet, with the thoroughness required to provide some guidance in estimating the increased OASPL over a corresponding steady jet. Hence, this study attempts to investigate the role of pulsation frequency and jet exit velocity on the near-field noise. The measurements were made over a range of subsonic jet Mach numbers and pulsing frequencies. Many of the parameters chosen here are consistent with those of Choutapalli [7].

### II. Experimental Techniques

#### A. Test Facility

The experiments were carried out in the pulsed-jet facility (Fig. 2) of the Advanced Aero Propulsion Laboratory located at the Florida State University. The facility was designed to produce pulsed jets at high subsonic Mach numbers with a stagnation temperature up to 800 K. High-pressure compressed air ($\sim$15 MPa) is stored in large storage tanks (10 $m^3$) and is used to drive the facility. The stagnation pressure and temperature in the settling chamber was maintained steady by a dome regulator combined with low pressure pneumatic valve and an inline flow through electrical heater with suitable controllers. The pressure and temperature were maintained to set conditions within a variation of $\pm$2 kPa and $\pm$0.5 K, respectively.

The settling chamber assembly housed a rotating disk used for chopping the flow. The rotational speed of the rotating disk was controlled by a DC motor (Baldor Smart Motor, model CSM3615T-2) through a shaft. The rotating disk ($D = 475$ mm) has six equally spaced circular holes with a nominal diameter of 76 mm. The pulsing frequency can be varied by changing the rotational speed of the

Received 24 June 2009; revision received 25 October 2009; accepted for publication 31 January 2010. 

*Research Scientist, College of Engineering, Department of Mechanical Engineering. Senior Member AIAA.
†Eminent Scholar and Professor, College of Engineering, Department of Mechanical Engineering.
‡Currently Assistant Professor, Department of Mechanical Engineering, University of Texas—Pan American. Member AIAA.

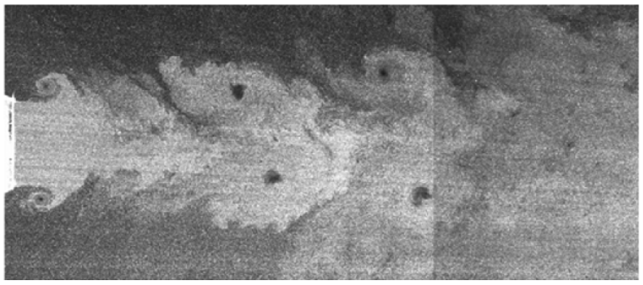

**Fig. 1 Schematic of the pulsed-jet flowfield (Choutapalli et al. [5]).**

motor. The frequency of pulsed flow and the rotational speed are related by

$$f(\text{Hz}) = \frac{\text{rotational speed (rpm)} \times 6}{60}$$

The endcap of the settling chamber has a circular hole of 76 mm. A 100-mm-long flexible stainless steel joint connects the opening of the endcap to a 228-mm-long straight smooth pipe, which in turn is connected to the nozzle inlet. The opening and closing of the rotating disk with respect to the flow result in the duty cycle of 50%. For the present study, a circular converging nozzle with an exit diameter $d = 50.8$ mm is connected to the facility. The interior contour of the nozzle is a fifth order polynomial converging smoothly from the 76 mm (pipe diameter) to the nozzle exit diameter ($d = 50.8$ mm). More details of the facility can be found in Choutapalli [7]. To minimize the sound reflections during the acoustic measurements, parts of the rig and nearby metal surfaces were covered with acoustic foam (Fig. 2).

### B. Measurements and Instrumentation

Near-field acoustic measurements were made using a 0.635-cm-diam ($\frac{1}{4}$-in.-diam) B&K condenser microphone (model 4939) array consists of 10 microphones, as shown in Fig. 3. These microphones have a relatively flat frequency response up to 100 kHz. The microphones were placed along an array parallel to the jet centerline, at 10 axial locations from $x/d = 0$ to 18 (where $x$ is the axial distance from the jet exit) with each microphone $2d$ apart. Measurements were made at three radial locations $5d$, $6d$, and $10d$ from the nozzle centerline, normal to the jet axis. The stagnation pressure is measured using an Omega pressure transducer (model PX215-100AI) in the straight pipe preceding the nozzle and was used to monitor the jet exit conditions. The pressure transducer was accurately calibrated using a RUSKA transducer before the measurements. Three B&K Nexus conditioning amplifiers (model 2690) were used for powering and conditioning microphone signals. Each channel of the B&K Nexus conditioner had built-in analog filter and has the capability of providing different gain settings. In the present experiments the microphone signals were conditioned using a low-pass filter set at 30 kHz. Depending upon the Mach number, different gain settings were used to obtain a high signal-to-noise ratio. The microphones were calibrated using a B&K piston phone (model 4220). This piston

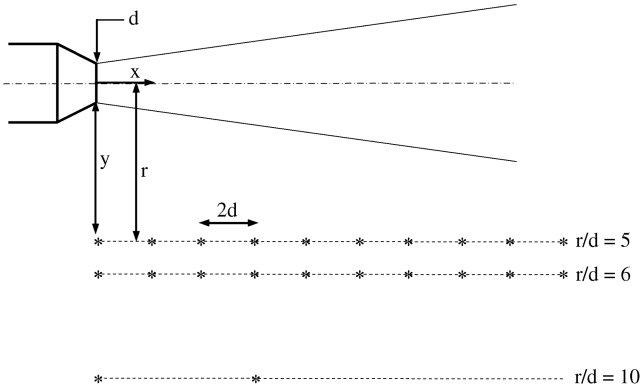


**Fig. 3 Locations of microphone array with respect to the jet.**

phone generates a known signal of 124 dB at a known frequency of 250 Hz. The correction values were then determined for each microphone and were used to correct the acquired signals before processing.

The pressure and acoustic signals were acquired using a high speed National Instruments digital data acquisition cards using LabVIEW$^{TM}$ and were processed offline. The microphone outputs were simultaneously sampled at a scan rate of 81,920 Hz. Standard fast Fourier transform analysis was used to obtain spectra and the OASPL from these measurements. A total of 1,638,400 samples were acquired to obtain statistically reliable narrowband spectra of 16,384 points each; this resulted in a narrow bandwidth of 5 Hz. The OASPL were measured with an accuracy of $\pm 0.5$ dB.

Flowfield data were obtained using particle image velocimetry (PIV). For PIV measurements, a dual-cavity digitally sequenced Nd:YAG laser (Spectra Physics PIV400) was used. A light sheet of 1 mm thickness was created by suitable combination of spherical and cylindrical lenses and the images were recorded simultaneously by two identical cross-correlation charge-coupled device cameras (SharpVision 1400–DE) fitted with 55 mm ($f2.8$) Nikon lenses. The resolution of the camera was $1.3k \times 1k$, which was operated in double-exposure mode. In the present experiments the jet was seeded with submicron ($\approx 0.3$ $\mu$m) oil droplets generated by a modified Wright nebulizer, which supplied the particles to the main jet. The ambient air was also seeded with smoke particles (1–10 $\mu$m) produced by a Rosco fog generator. More details on PIV measurements can be found in Choutapalli et al. [5]

### C. Test Conditions

The experiments were conducted at jet exit Mach numbers of 0.3, 0.5, 0.7, and 0.8. The pulsing frequency ($f$) was varied from 0–220 Hz for each Mach number. For $M = 0.3$, the Strouhal number ($St = fd/U_j$, where $f$ is the pulsing frequency, $D$ is the nozzle exit diameter, and $U_j$ is the nozzle exit mean velocity) varied from 0–0.106. Because of the facility limitations, the maximum pulsing frequency is limited to 220 Hz. As a result, with increasing jet exit Mach numbers, the $St$ number range will be reduced. The steady-jet condition is referred to here as $St = 0$. A typical unsteady total

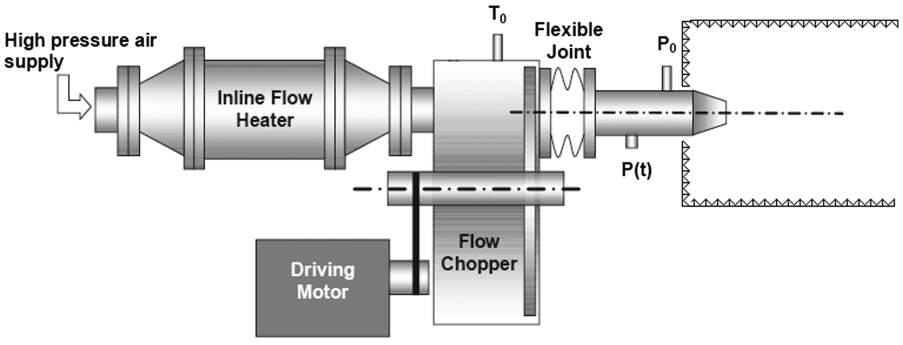


**Fig. 2 Schematic of the test facility.**

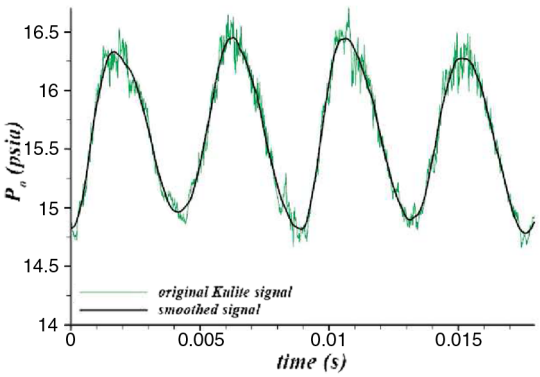


**Fig. 4 Total pressure variations with time at the center of nozzle exit; $St = 0.106$ and $M = 0.3$.**

pressure time signal measured using a Kulite transducer (model no. XCE 062-100A) incorporated into a total pressure probe (diameter = 1.6 mm) at the center of the nozzle exit is shown in Fig. 4. The solid line in the figure is a smoothing signal shown only to guide the eye through the data points. The nearly sinusoidal variation of the nozzle exit flow is depicted in the pressure time signal. The periodicity in the signal at the pulsing frequency is maintained at all the measurement locations (up to a distance of $x/d = 18$, [14]).

The variation of the normalized pressure fluctuation intensity ($p_{\text{rms}}$) with frequency for $M = 0.3$ and 0.8 are shown in Fig. 5. For a given Mach number, the amplitude variation with frequency is relatively small. With increasing Mach number, the fluctuation amplitude is decreased. For example, at $M = 0.3$, the normalized rms intensity assumes a nominal value of 0.55 as compared with 0.45 at $M = 0.8$. The jet stagnation temperature was kept constant at 300 K. A top-hat mean exit velocity profile with turbulent boundary layer is observed at the nozzle exit (Choutapalli et al. [5]). The Reynolds number based on mean jet exit velocity and nozzle diameter varied from $3.25 \times 10^5$ to $9.2 \times 10^5$.

### D. Results and Discussion

The focus of the present study is to characterize the near-field noise of a pulsed jet and to study the effect of important parameters such as jet Mach number and pulsing frequency. This is examined in terms of overall sound pressure levels and pressure spectra at various test conditions. In this Note we present typical results and the related discussion; the results at other test conditions can be found in Kumar et al. [14].

#### 1. *Steady Jet*

To characterize the noise of a pulsed jet, it is important to measure the noise characteristics of a corresponding steady jet. The

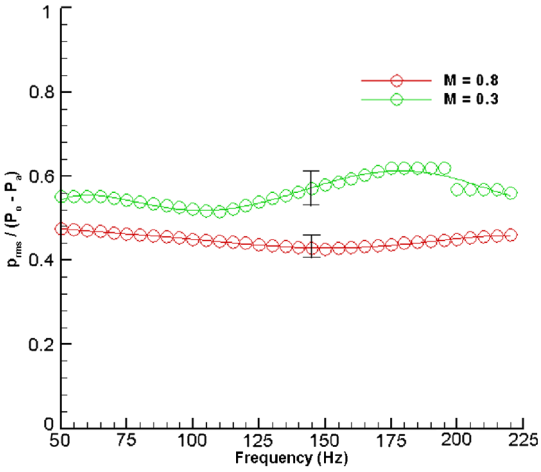


**Fig. 5 Variation of normalized pressure fluctuation with pulsing frequency.**

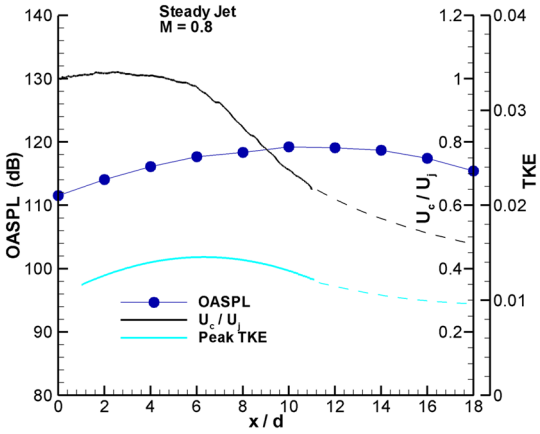


**Fig. 6 Noise and flowfield characteristics of a steady jet.**

measurements were made at four Mach numbers of 0.3, 0.5, 0.7, and 0.8 without pulsing the jet. Figure 6 shows the variation of the centerline mean axial velocity (normalized with mean jet exit velocity), peak turbulent kinetic energy (TKE = $1/2(\bar{u}'^2 + \bar{v}'^2)$) and near-field OASPL with downstream distance. The TKE presented here are taken in the central plane of the jet. However, the three-dimensional PIV measurements made in a cross plane at $x/d = 10$ indicate that the two transverse components ($v'$ and $w'$) show nearly equal rms magnitude [7]. The solid line represents the PIV data, and the dotted line is based on other measurements in the literature (Arakeri et al. [8] and Lau et al. [15]). The peak turbulent intensities in subsonic jets near the nozzle exit are typically found along the nozzle lip line and away from the jet centerline. The values of TKE presented here are the peak levels in the shear layer of the jet; however, downstream of potential core the highest levels of TKE can exist near the centerline of the jet. The noise measurements in the near field are likely to be affected by the jet spreading. Hence, the fixed radial position microphone array measurements for both steady and pulsed jets are corrected for jet spreading by linear interpolation of data obtained at various radial locations; the information on the jet spreading rate for both steady and pulsed jets was taken from [7]. In this fashion, the OASPL represents microphone locations that are equidistant from the jet edge and correspond to a microphone array placed at $y/d = 4.5$ (where $y$ is the radial distance of the microphone from the jet boundary). While the peak TKE in the shear layer is reached just beyond the potential core of the jet, the OASPL continue to increase further downstream. Peak OASPL are observed at $x/d = 14$ and $\approx 10$ for $M = 0.3$ and 0.8, respectively. Within the measurement region, the OASPL varied about 10 dB with observed maxima of 100 and 120 dB for $M = 0.3$ and 0.8, respectively.

The narrowband near-field frequency spectra for the steady jet at different Mach numbers are shown in Fig. 7. The spectra cover a

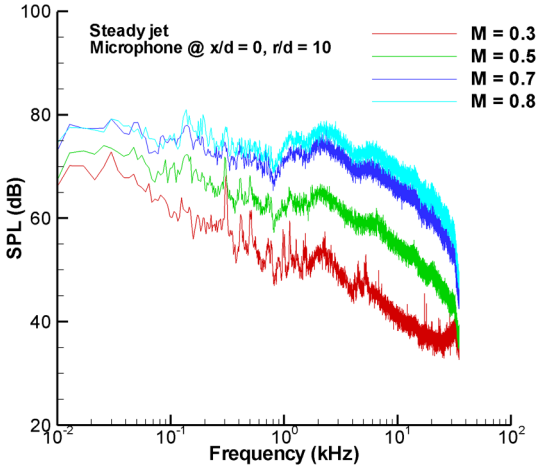


**Fig. 7 Effect of Mach number on the steady-jet noise spectra.**

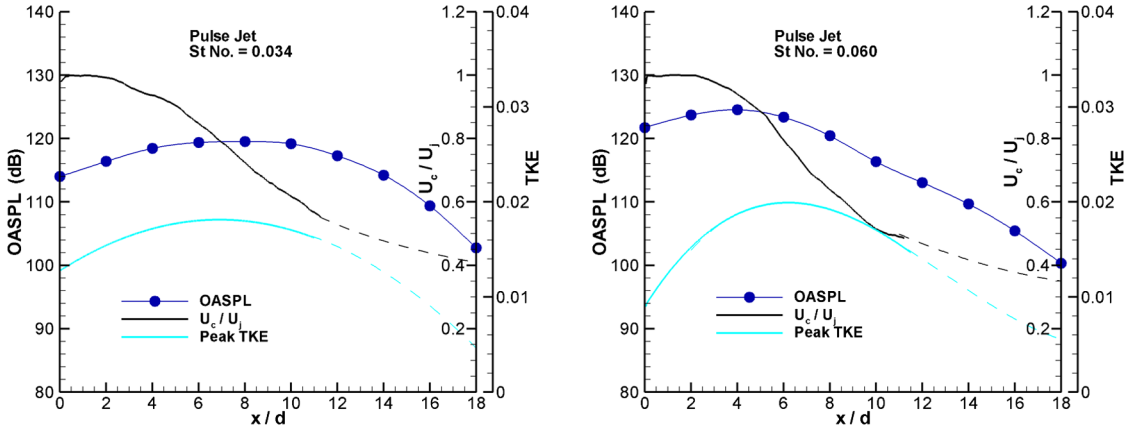


**Fig. 8 Noise and flowfield characteristics of a pulsed jet.**

frequency range from 10 Hz to 30 kHz. The spectra correspond to a radial location of $r/d = 10$ and $x/d = 0$. As generally observed, the sound pressure levels (SPL) increase with increase in jet Mach number, with the spectra displaying its broadband nature without any dominant peaks. With increasing Mach number, higher frequencies become prominent. For example, at $M = 0.8$, frequencies up to about 10 kHz show relatively high SPL.

### 2. *Pulsed Jet*

Figure 8 shows the pulsed-jet data at conditions similar to that of a steady jet shown in Fig. 6. Two Strouhal number ($St$) cases at $M = 0.3$ are considered for discussion. The variation of OASPL with downstream distance is in accord with the peak TKE distribution. Peak OASPL are observed at $x/d = 8$ and $\approx 4$ for $St = 0.034$ and 0.06, respectively, with corresponding values of 120 and 125 dB. The upstream shift in the peak OASPL with increasing $St$ is in conformity with the peak TKE behavior. Figure 9 shows the downstream variation of the vortex ring circulation for three different $St$. As can be seen from the figure, that the circulation peak locations ($x/D = 8$ for $St = 0.034$ and $x/d = 4$ for $St = 0.06$) are identical to those found in the OASPL variation in Fig. 8. Therefore, it is suggested that the peak OASPL in the near field occurs at a location where the vortex ring achieves its maximum circulation. It is also found that with increasing $St$, the OASPL increases, as shown in Fig. 10. The ordinate ($\Delta$dB) is the difference between the OASPL values of the pulsed jet and the corresponding steady jet at $x/d = 0$ and $r/d = 10$. Included in the figure are the data corresponding to all four Mach numbers and a range of frequencies from 0–220 Hz. For the range of parameters tested, a maximum OASPL increase of about 32 dB is observed. It is interesting to observe that $\Delta$dB assumes a unique behavior with Strouhal number.

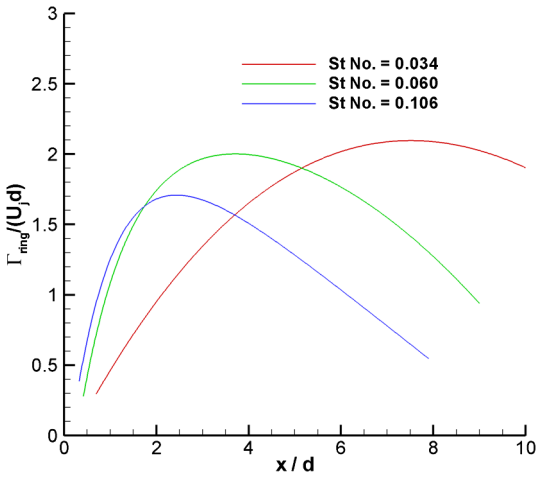


**Fig. 9 Variation of vortex ring circulation [7].**

Figure 11 shows the effect of jet exit Mach number on the near-field frequency spectra measured in the jet exit plane at a fixed radial location ($r/d = 5$). The case of pulsing frequency $f = 100$ Hz are considered here. As envisaged, the spectra show distinct peaks corresponding to the pulsing frequency and its harmonics. The primary tone has amplitude of about 40 dB over the background noise. At low frequencies, where the tones are prominent, the spectra indicate little influence of Mach number. While at higher frequencies, the spectra behave in a fashion similar to that of the steady jet (Fig. 6). This low-frequency behavior can be attributed to the broadband amplification that usually occurs when strong tones are present in the spectra [16]. The spectra at other pulsing frequencies show very similar behavior to that seen at a pulsing

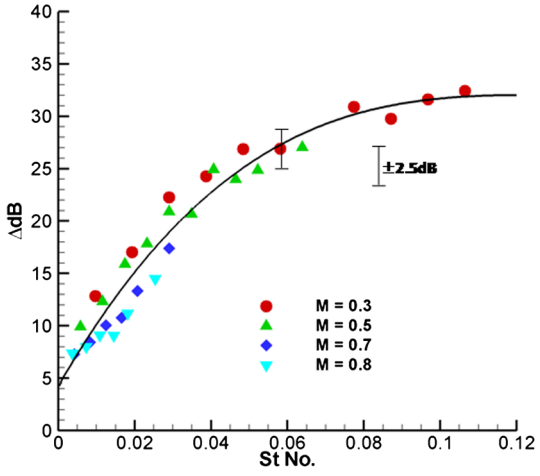


**Fig. 10 Increase in OASPL with Strouhal number, $x/d = 0$, $r/d = 10$, and $M = 0.3$–$0.8$.**

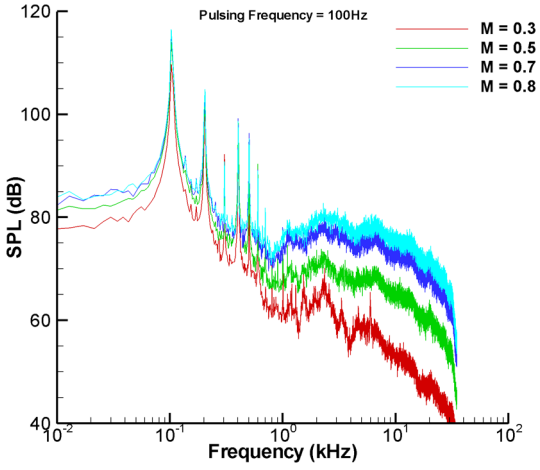


**Fig. 11 Effect of Mach number on the pulsed-jet noise spectra.**

frequency of 100 Hz, except that the dominant tones shift as the pulsing frequency changes [14].

## III. Conclusions

A pulsed-jet flowfield is generally described as a series of vortex rings interspersed by jetlike flows. Depending upon the pulsing frequency, the jet flow between the rings can be absent. The interest in this Note is the sound generated by the pulsed jet within the first few (less than 20) diameters of where most of the large-scale energetic vortices exist. The presence of such vortices is known to produce noise that is not well understood. As a result, this experimental study focuses on obtaining near-field noise characteristics of a pulsed jet. The pulsed-jet conditions are similar to those of Choutapalli [7], who obtained detailed flow measurements. The noise measurements are confined to radial locations that are less than 10 diameters from the jet centerline.

A substantial increase in the near-field OASPL over the corresponding steady jet is observed with pulsed jets. The variation of $\Delta$dB ($\mathrm{OASPL}_{\mathrm{pulsed\ jet}} - \mathrm{OASPL}_{\mathrm{steady\ jet}}$) with Strouhal number assumes a universal character. For the range of parameters tested, a maximum increase of 32 dB increase is observed at $St \geq 0.1$.

In the near field, the peak OASPL is observed at a downstream location where the vortices assume maximum circulation. The pressure spectra of pulsed jets feature large-amplitude tone corresponding to pulsing frequency and its harmonics. These tones help to increase the broadband SPL at low frequencies through a commonly known phenomenon of broadband amplification due to the presence of strong tones.

## References

[1] Gharib, M., Rambod, E., Kheradvar, A., Shan, D. J., and Dabiri, J. O., "*Optimal Vortex Formation as an Index of Cardiac Health*," *Proceedings of the National Academy of Sciences*, Vol. 103, No. 16, April 2006, pp. 6305–6308. doi:10.1073/pnas.0600520103

[2] Manganiello, E. J., Valerino, M. F., and Essig, R. H., "Sea-Level Performance Tests of a 22-Inch Diameter Pulse Jet," NACA Rept. E5J02, 1945.

[3] Seikmann, J., "On The Pulsating Jet from the End of a Tube, with Application to the Propulsion of Certain Aquatic Animals," *Journal of Fluid Mechanics*, Vol. 15, 1963, pp. 399–418. doi:10.1017/S0022112063000331

[4] Weihs, D., "Periodic Jet Propulsion of Aquatic Creatures," *Fortschritte der Zoologie*, Vol. 24, 1977, pp. 171–175.

[5] Choutapalli, I., Krothapalli, A., and Arakeri, J. H., "An Experimental Study of a Turbulent Pulse Jet," *Journal of Fluid Mechanics*, Vol. 631, 2009, pp. 23–63. doi:10.1017/S0022112009007009

[6] Crow, S., and Champagne, F., "Orderly Structures in Jet Turbulence," *Journal of Fluid Mechanics*, Vol. 48, 1971, pp. 547–591. doi:10.1017/S0022112071001745

[7] Choutapalli, I. M., "An Experimental Study of a Pulsed Jet Ejector," Ph.D. Thesis, Florida State Univ., Tallahassee, FL, 2006.

[8] Arakeri, V. H., Krothapalli, A., Siddavaram, V., Alkislar, M. B., and Lourenco, L. M., "On the Use of Microjets to Suppress Turbulence in a Mach 0.9 Axisymmetric Jet," *Journal of Fluid Mechanics*, Vol. 490, 2003, pp. 75–98. doi:10.1017/S0022112003005202

[9] Mollo-Chirstensen, E., "Jet Noise and Shear Flow Stability Seen from an Experimenter's Viewpoint," *Journal of Applied Mechanics*, Vol. 34, 1967, pp. 1–7.

[10] Alkislar, M. B., Krothapalli, A., and Lourenco, L. M., "Structure of a Screeching Rectangular Jet: A Stereoscopic PIV Study," *Journal of Fluid Mechanics*, Vol. 489, 2003, pp. 121–154. doi:10.1017/S0022112003005032

[11] Hooker, R. J., and Rumble, R. H., "Noise Characteristics of a Pulsed Jet," *Noise Control Engineering*, Vol. 17, No. 3, 1981, pp. 113–119. doi:10.3397/1.2832192

[12] He, X., and Karagozian, A. R., "Performance and Noise Characteristics of Pulse Detonation Engine," AIAA Paper 2004-469, Jan. 2004.

[13] Shaw, L., Harris, K., Schauer, F., and Hoke, J., "Acoustic Measurements for a Pulse Detonation Engine," AIAA Paper 2005-2952, May 2005.

[14] Kumar, R., Krothapalli, A., and Greska, B., "Near-Field Noise Characteristics of a Pulse Jet," AIAA Paper 2008-3030, May 2008.

[15] Lau, J. C., Morris, P. J., and Fisher, M. J., "Measurements in Subsonic and Supersonic Free Jets Using a Laser Velocimeter," *Journal of Fluid Mechanics*, Vol. 93, 1979, pp. 1–27. doi:10.1017/S0022112079001750

[16] Moore, C. J., "The Role of Shear-Layer Instability Waves in Jet Exhaust Noise," *Journal of Fluid Mechanics*, Vol. 80, 1977, pp. 321–367. doi:10.1017/S0022112077001700

M. Glauser
*Associate Editor*